Check for updates

EurJIC
European Journal of Inorganic Chemistry

Chemistry Europe
European Chemical Societies Publishing

Accepted Article

Title: A bis-polydentate oxamate-based achiral ligand able to stabilize a macrocyclic mixed valence compound or induce a 1D helical chain

Authors: Ang Li, Yanling Li, Lise-Marie Chamoreau, Christophe Desmarets, laurent lisnard, and Yves Journaux

This manuscript has been accepted after peer review and appears as an Accepted Article online prior to editing, proofing, and formal publication of the final Version of Record (VoR). This work is currently citable by using the Digital Object Identifier (DOI) given below. The VoR will be published online in Early View as soon as possible and may be different to this Accepted Article as a result of editing. Readers should obtain the VoR from the journal website shown below when it is published to ensure accuracy of information. The authors are responsible for the content of this Accepted Article.

To be cited as: *Eur. J. Inorg. Chem.* 10.1002/ejic.202000490

Link to VoR: https://doi.org/10.1002/ejic.202000490

WILEY-VCH

10.1002/ejic.202000490

WILEY-VCH

A bis-polydentate oxamate-based achiral ligand able to stabilize a macrocyclic mixed valence compound or induce a 1D helical chain

Ang Li,[a] Yanling Li,[a] Lise-Marie Chamoreau,[a] Christophe Desmarets,[a] Laurent Lisnard,*[a] and Yves Journaux*[a]

Abstract: The reaction of the *N*-(2-hydroxyphenyl)oxamate ligand (ohpma) has been investigated with cobalt(II) and copper(II) ions. It has led to two coordination compounds, $(TMA)_3[\{Co^{III}(ohpma)_2Co^{II}(MeOH)_2\}_3]\cdot 10H_2O\cdot 5MeOH$ (**1**) and $(HNEt_3)[Cu(ohpma)]$ (**2**). Both compounds have been characterized by single-crystal X-ray diffraction and magnetometry. The X-ray diffraction studies have revealed atypical structures that are not commonly observed in oxamate coordination chemistry with a macrocyclic arrangement for the mixed-valence cobalt-based complex **1**, and a helical chiral chain for compound **2**. In the latter, the bis-polydentate nature of the $(ohpma)^{3-}$ ligand with distinct tridentate and bidentate coordination sites creates a chirogenic center on the copper ion. The investigation of the magnetic properties shows for complex **1** a single-molecule magnet behavior detectable under static field, while antiferromagnetic interactions dominate the behavior of **2**.

Introduction

Oxamate ligands have largely proven their efficiency for the design of metalloligands and the rational multi-step preparation of attractive molecular materials, from sensors, sieves and chemical nanoreactors to magnets and spintronic candidates.[1–6] This is undoubtedly related to their chemical flexibility and the wide range of organic substrates that can yield oxamate ligands. Considerable work has been devoted so far to phenyl-based oxamate ligands, and more recently, amino acid-based oxamate ligands have also shown strong appeal.[7–13] In the case of phenyl derivatives, the role of alkyl substituents and their steric hindrance has also been probed to investigate the effect on the magnetic interactions and on the dimensionality of the compounds.[14–16] The introduction on the phenyl ring of additional coordinating groups to afford *multi*-polydentate ligands is, however, less investigated. Some phenyloxamate-based ligands bearing additional carboxylato or hydroxo groups, or else pyridine-based oxamate ligands, have been successfully prepared and used to coordinate metal ions.[17–26] Nevertheless, their study has either been focused on the metalloligand formation or been limited by deprotonation issues, preventing the "full" coordination of such multi-polydentate ligands. So far, only two ligands have been observed to display a coordination mode where all donor atoms participate at least in one coordination bond: the 2-(oxamato)benzoic acid and the 2,6-pyridinebis(oxamic acid).[18,23]

Seeking to explore the reactivity of these multi-polydentate oxamate-based ligands, we have been investigating the ethyl *N*-(2-hydroxyphenyl)oxamate ligand (H_2Et-ohpma, Figure 1) and we present here two coordination compounds obtained by its reaction with Co(II) or Cu(II) ions: the macrocyclic complex $(TMA)_3[\{Co^{III}(ohpma)_2Co^{II}(MeOH)_2\}_3]\cdot 10H_2O\cdot 5MeOH$ (**1**) and the chiral one-dimensional polymer $(HNEt_3)[Cu(ohpma)]$ (**2**). The compounds have been obtained in non-aqueous media starting from the ester oxamate ligand or its acid, and while a chloride salt of the copper(II) ions was used to prepare **2**, a carboxylate cobalt(II) starting materials was necessary to isolate complex **1**. Both compounds display uncommon structural types for oxamate-based systems. The characterization of the magnetic properties also revealed that **1** behaves as a single-molecule magnet.

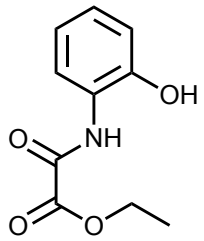

Figure 1. Representation of the H_2Et-ohpma ligand.

Results and Discussion

Crystal structures. Complex **1** crystalizes in the monoclinic $P2_1/c$ space group and consists of an anionic hexametallic mixed-valence $\{Co^{III}_3Co^{II}_3\}$ macrocyclic ring-like complex (Figure 2). In the ring, three Co^{II} ions are bridged by three bis-bidentate $[Co^{III}(ohpma)_2]^{3-}$ complexes. In the $[Co^{III}(ohpma)_2]^{3-}$ complex, the Co^{III} ion is coordinated to two $(ohpma)^{3-}$ ligands, via their tridentate sides involving the nitrogen and oxygen atoms of the oxamato groups, and the oxygen atoms of the phenolato group. The Co^{III} ion is thus six-coordinate in an octahedral geometry.

[a] Dr. A. Li, Dr. Y. Li, L.-M. Chamoreau, Dr. C. Desmarets, Dr. L. Lisnard, Dr. Y. Journaux
Sorbonne Université, CNRS, Institut Parisien de Chimie Moléculaire, IPCM, F-75252, Paris, France
E-mail: laurent.lisnard@sorbonne-universite.fr
Homepage: www.ipcm.fr

Supporting information for this article is given via a link at the end of the document.

Accepted Manuscript

This article is protected by copyright. All rights reserved.

Co^{III}-N/O bond lengths vary from 1.870(6) to 1.967(4) Å (*av.* 1.907 Å). Angles in the octahedral geometry around the metal center vary from 83 to 98° (average deviation from orthogonality of 4°) and the O-Co-O angles indicative of the ligands' constraint vary from 169 to 171°. The Co^{II} ions are six-coordinate in distorted octahedral environments (two of the Co^{II} atoms are disordered, see experimental section). Each ion is coordinated to two $[Co^{III}(ohpma)_2]^{3-}$ complexes via their remaining carbonyl oxygen atoms, and to two methanol solvent molecules. Co^{II}-O distances vary from 2.041(6) to 2.181(5) Å (*av.* 2.095 Å), and the O-Co-O angles from 80 to 100° (*av.* deviation to orthogonality of 5°). BVS calculations support the presence as well as the localisation within the ring of both Co^{II} and Co^{III} ions (see supporting information). The oxidation of the cobalt ions must result from the coordination by the $(ohpma)^{3-}$ ligand in basic medium and in air.

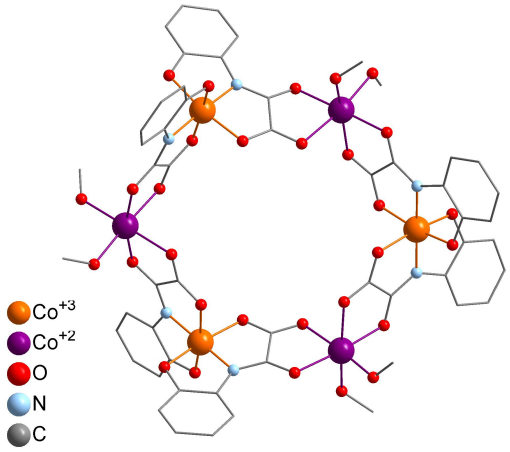

Figure 2. Structure representation of **1**. Solvent molecules, TMA^+ cations and H atoms have been omitted for clarity.

In the solid, the TMA^+ cations are located between the rings, and relatively strong H-bonds (O···O < 2.6 Å) between coordinated methanol molecules and oxygen atoms from the phenolato groups generate chains of macrocycles along the crystallographic *b* axis (Figure S1 in the supporting information). The shortest intermolecular metal-metal distance is actually situated along the H-bond between Co^{II} and Co^{III} ions, and is of 5.73 Å. Considering paramagnetic ions, the shortest intermolecular distance is also found between two adjacent rings in the chain, and it is equal to 6.76 Å.

Complex **1** is only the third example of oxamate-based coordination ring. The other two examples being a Cu^{II} hexametallic wheel, which is based on an amino-acid-based oxamate ligand,[27] and a decametallic $\{Mn^{II}_5Cu^{II}_5\}$ wheel obtained from a bis-oxamate ligand.[28] If the hexagonal ring structure was unexpected, it seems, in hindsight, a logical outcome. From a thermodynamic point of view, an octahedral cobalt complex with two tridentate ligands should be more stable and form preferentially. The presence of two deprotonated amide functions in the coordination sphere of the cobalt ion also makes this complex easier to oxidize. It is well established that deprotonated amide function stabilize metal ions in high oxidation states.[29–32] As this Co(III) complex will be inert, its formation should constitute the first step in the building of the hexagonal ring. It places the two uncoordinated bidentate parts of the two oxamato ligands at 120° from each other. This arrangement makes the formation of hexagonal cycles or zigzag chains highly probable when $[Co^{III}(ohpma)_2]^3$ complexes coordinate with Co(II) ions.

Compound **2** consists of an anionic oxamato-bridged Cu^{II} helical chain with triethylammonium counter-cations. It crystallizes in the trigonal $P3_2$ chiral space group. In the chain, the Cu^{II} ion is five-coordinate and adopts a square-based pyramid geometry. The base is defined by one nitrogen and two oxygen atoms coming from the phenolato and oxamato groups of the ligand (N1, O1, O4), and one oxygen atom (O3) from a second oxamate function belonging to bidentate side of an adjacent ligand. The latter has its remaining carbonyl oxygen atom (O2) occupying the apical position of the Cu^{II} complex (Figure 3). The bond lengths around the copper atom (in Å: Cu-N1 = 1.914(2), Cu-O3 = 1.965(2), Cu-O4 = 1.969(1), Cu1-O1 = 1.983(1), Cu1-O2 = 2.243(1)) are rather short looking at the Cu-N(amide) and Cu-O(carboxylate) bonds formed with the oxamato group. It resembles that of more constrained oxamate-based complexes, such as those obtained with bis-oxamate ligand (from 1.887 Å to 1.931 Å),[33–38] in opposition to bis(mono-oxamate) Cu^{II} complexes.[39–41] The O1-Cu-O4 angle from the phenolate to the oxamate group is a good indicator of the constraint coming from the tridentate side of the ligand, with a value here of 162°.

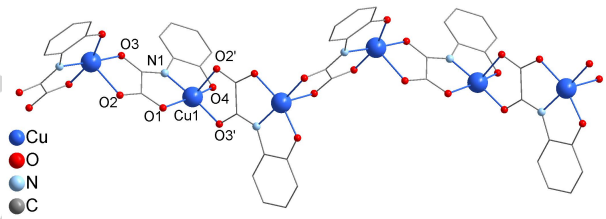

Figure 3. Structure representation of **2** with atom labels. $HNEt_3^+$ cations and H atoms have been omitted for clarity.

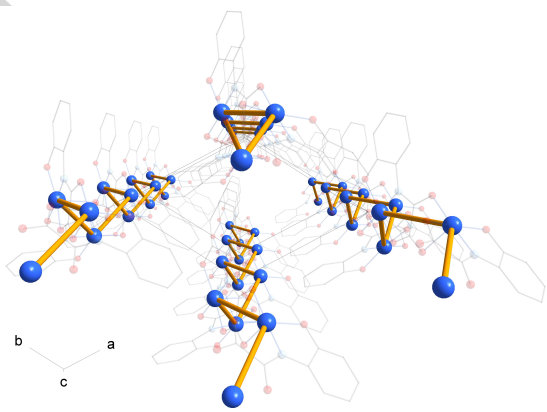

Figure 4. Representation of the helices in the packing of **2**, through the intrachain Cu—Cu bonds (orange). $HNEt_3^+$ cations and H atoms have been omitted for clarity.

Accepted Manuscript

This article is protected by copyright. All rights reserved.

Interestingly, this 1D chain has a helical configuration (Figure 4), which is rarely observed in oxamate chemistry.[42,43] The two other examples of helical chains have been observed both with copper ions, and with an amino-acid-based oxamate ligand, (R)-*N*-(ethyloxoacetate)phenylglycine, or the 2-dimethylaminoethyl(oxamate) ligand. Indeed, these ligands have very similar tridentate coordination modes with donor atoms on the β-carbon of the *N*-substituted oxamato group.

Compound **2** grows parallel to the crystallographic *c* axis and the chains are rather well separated from each other (Figure 4, and Figures S2-S3 in the supporting information). The helical configuration along with the peripheral phenyl groups from the ligands and the bulky triethylammonium cations afford an effective spacing between the metal ions of neighboring chains. The shortest interchain Cu···Cu distance is 9.66 Å.

This 1D chain adopts a left-handed configuration. None of the tested crystals crystallize in the enantiomorphic $P3_1$ space group. The solid state circular dichroism (CD) and absorption spectra of **2** are shown in Figure 5. The CD spectrum of **2** exhibits a pair of weak positive peaks at 280 nm and 314 nm, and a negative Cotton effect around 280 (strong), 386 (strong) and 775 nm (weak). The investigation of several batches of compound **2** with CD measurements in the solid state indicates that the left-handed helicity is the only configuration we observe, while the synthesis solution gives no dichroic signal (see supporting information, Figures S4-S6).

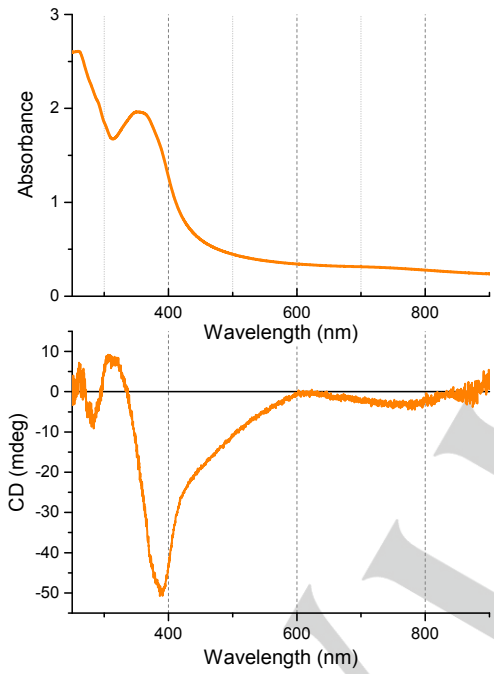

Figure 5. UV-Vis and CD spectra of compound **2** in the solid state (pellet; 0.25 % in KBr).

Spontaneous resolution is not a frequent phenomenon.[44] It is even less common when the reactants are achiral. For coordination polymers, the helical structure is generally obtained with flexible or atropisomeric ligands able to induce a pitch angle due to ligand torsion or the rotation around a C-C bond.[45] The helical structure and pitch of the helix are then induced by interchain interactions. These are difficult to control and it is almost impossible to predict whether a helical structure will be obtained. It is worthy of note that the $(ohpma)^{3-}$ ligand is not atropisomeric, and that the existence of a helical structure cannot come from the ligand. In fact, it is the bis-polydentate nature of the $(ohpma)^{3-}$ ligand associated to the 4+1 coordination of the copper ions that induce the helicity in compound **2**. The bis-polydentate $(ohpma)^{3-}$ ligand acts as a tridentate ligand on one side and as a bidentate ligand on the other. The base of the square pyramidal coordination of the Cu(II) ions in **2** is determined by the tridendate side of the $(ohpma)^{3-}$ ligand with the remaining corner being occupied by one oxygen atom from the bidentate side of an adjacent $(ohpma)^{3-}$ ligand. This means that the oxamate group of the tridentate part of the ligand occupies one edge of the square base while the two oxygen atoms of the bidentate part of the neighboring oxamate ligand occupy one edge on the *opposite* triangular face of the pyramid (Figure 6). For a pyramid whose height is equal to one half of the square diagonal, there is a 120° angle between the two directions described by these edges. As the copper-copper directions are perpendicular to these edges, this configuration determines the 120° angle formed by three successive copper ions (Figure 6).

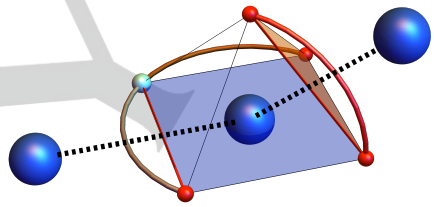

Figure 6. Representation of the 4+1 coordination sphere of the copper ions, with the 120° "right edge" (see text) linking between successive copper ions (blue copper ions, red oxygen atoms, light blue nitrogen atom). The polyhedron edges in red symbolize the position of the oxamate groups in the coordination sphere.

In fact, the asymmetric nature of the chelation in this ligand, tridentate on one side and bidentate on the other, creates a chirogenic center on the Cu(II) ion with no inversion center or mirror. In **2**, the connection between adjacent copper ions is always made via the right edge of the triangular face that sits opposite the oxamate group lying in the square base of a complex. This confers a SPY-5-14(A) absolute configuration for the Cu ions,[46] and the chaining results in a left-handed helicity. The angle of 120° determines a pitch of three for the helical structure (the *c* axis value). A chaining through the left edge of the pyramid triangular face would lead to a right-handed helical structure and to the $P3_1$ space group. The other possible and simple arrangement would be a regular alternation of "left edge" (SPY-5-14(C) configuration) and "right edge" (SPY-5-14(A) configuration) connectivities in the pyramid triangular face, resulting in a cyclic hexagonal structure (Figure S7 in the supporting information). Less simple sequences of connections would lead to other types of structures that are more difficult to anticipate.

Accepted Manuscript

This article is protected by copyright. All rights reserved.

Compound **2** is not the first example of a helical chain with magnetic ions obtained from non-chiral reactants. The most emblematic examples are the metal nitronyl nitroxyde chains which include the first reported single-chain magnet.[47–49] However, the use of copper ions and substituted oxamate ligands that offer a tridentate side at either end of the oxamate bridge seems to make the preparation of helical chains almost controllable. As explained above, the number of likely structures is reduced, with the most probable ones being the hexagonal macrocycle and the helical chain. This is well illustrated by the work of Pardo *et al.* with oxamate ligands that are substituted with chiral amino acid.[27,43]. With R or S-valine substituted oxamate ligands, they have obtained hexametallic copper(II) wheels where the copper ions alternate the left edge (SPY-5-12(C) configuration) and right edge (SPY-5-12(A) configuration) connectivities on the pyramid triangular face.[27] Whereas the use of the D-phenyl-glycine substituted oxamate ligand yields a right-handed helical chain crystallizing in the $P3_1$ space group. In this structure, it is always the left edge of the pyramid's triangular face that links neighboring copper ions (SPY-5-12(C) configuration).[43] The structure of compound **2** and the results obtained by Pardo *et al.* show that the use of a bidentate/tridentate double-sided oxamate-based ligand and the 4+1 coordination of Cu(II) ions can induce helical or cyclic structure. This is supported by the early work of Kachi-Terajima *et al.* They have obtained with the achiral 2-dimethylaminoethyl(oxamato) ligand and Cu(II) ions a left-handed helical chain. As in compound **2**, the chain forms through the right edge connectivity of the pyramid's triangular face, leading to an absolute SPY-5-13(C) configuration.[42] However, it is puzzling that all the tested crystals give the same left-handed helicity whereas, with an achiral ligand in a case of spontaneous resolution, a conglomerate with the same amount of crystals of both enantiomers is expected. Kachi-Terajima *et al.* describe the same phenomenon with equally no satisfactory explanation.[42] This enantiomeric excess has also been observed by other authors in the case of spontaneous resolution.[50] It has been shown that an enantiomeric excess can be induced by various means such as agitation[51] or a competitive reaction.[52] Similarly, it can be suppressed in some cases by sonication of the reagents.[50] A possible explanation for compound **2** could be the existence of a very fast equilibrium in solution between the two enantiomers which favors the crystallization of an enantiomer as soon as it starts to crystallize.[53] In this case, however, the enantiomer obtained should vary from one crystallization to the other and this is not what we observe. At this stage, we thus lack a satisfactory explanation for obtaining only the left-handed helicity.

The magnetic properties of complex **1** were studied under a field of 500 Oe and in a 3-200 K temperature range, shown by the $\chi_M T$ versus T plot in Figure 7. At 200 K, the $\chi_M T$ value is 9.71 $cm^3\ mol^{-1}$ K and it sits in the expected range for three isolated Co^{II} ions ($2.7 < \chi_M T < 3.4$ $cm^3 mol^{-1} K$ for one Co(II),[54] so $8.1 < \chi_M T < 10.2$). Upon cooling, $\chi_M T$ steadily decreases to reach a value of 5.64 $cm^3\ mol^{-1}$ K at 13 K. The product then goes up before finally decreasing to 5.18 $cm^3\ mol^{-1}$ K at 3 K. Down to 13 K, this behavior is typical of Co(II) ions in octahedral environment with a $^4T_{1g}$ ground state and first order spin-orbit coupling. The bump of $\chi_M T$ curve around 12 K is caused by the non stoichiometric hydrated cobalt hydroxide impurity which is commonly seen around 10−15 K in Co^{II} complexes when performing low field measurements (Figure 7).[55]

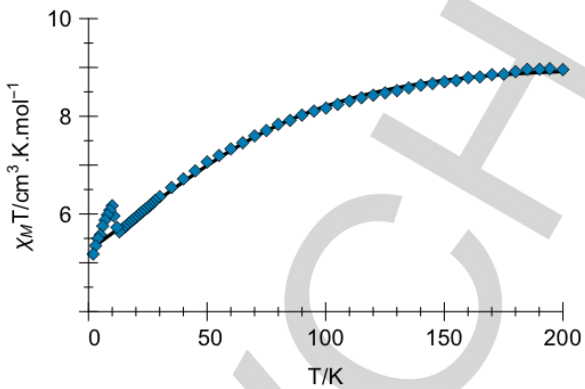

Figure 7. Temperature dependence of $c_M T$ for **1** under an applied magnetic field of 500 Oe from 3 to 200K. The solid black line is the best obtained fit.

The interaction between the Co^{II} ions through the diamagnetic Co^{III} metalloligands within the ring is expected to be very small and the magnetic data can be modeled as three isolated Co^{II} ions using the following Hamiltonian and the T≡P isomorphism:[56–58]

$$H^{\upsilon} = \sum_{i=1}^{3}\left[-\frac{3}{2}\alpha\lambda L_{Co_i} S_{Co_i} + \Delta\left(L^2_{zCo_i} - \frac{1}{3}L^2_{Co_i}\right) + \left(-\frac{3\alpha}{2}L_{\upsilon Co_i} + g_e S_{\upsilon Co_i}\right)\beta.H\right]$$

with υ = x, y, z

λ is the spin-orbit coupling constant, α the orbital reduction factor and Δ the axial distortion parameter. L and S are respectively the orbital and spin operators with L = 1 in the T-P isomorphism approach and S = 3/2. The least square fit of the magnetic data in the 200-13 K temperature range gave λ = -132 cm^{-1}, α = 0.84, Δ = -378 cm^{-1}, with an agreement factor F = $2.6*10^{-5}$ calculated as follows:

$$F = \frac{\sum\left[(\chi_M T)_{exp} - (\chi_M T)_{calc.}\right]^2}{\sum\left[(\chi_M T)_{exp}\right]^2}$$

The dynamic properties of **1** were explored by alternating-current measurements (AC). At zero DC magnetic field, there were neither frequency-dependent χ_M' nor χ_M'' signals observed and it may come from the fast quantum tunneling effect reported in other single-ion or single-molecule magnets (SIMs and SMMs).[59,60] However, when DC magnetic field is applied, both the χ_M' and χ_M'' gave strong frequency dependent signals typical of SMMs. The measurements shown in Figure 8 were performed under a 1800 Oe DC field that was determined to maximize relaxation time. Nevertheless, the blocking temperature is quite low and the maxima of χ_M' and χ_M'' are only visible at high frequency.

To extract the relaxation times, the generalized Debye model, which considers a distribution of relaxation times, has been used.[61]

Accepted Manuscript

This article is protected by copyright. All rights reserved.

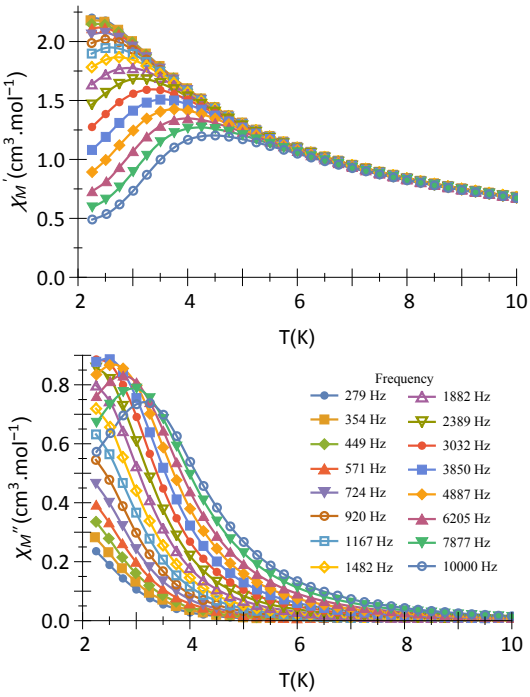

Figure 8. Temperature dependence of χ_M' (a) and χ_M'' (b) in **1** under an applied DC field of 1800 Oe and in the 10−10000Hz frequency range. The solid lines are only eye-guides.

The frequency dependence of χ_M'' and Cole-Cole plot of **1** are shown in Figure 9. As suggested by Dekker *et al.*,[62] two steps procedures were used to extract the relaxation time τ at each temperature. First a fit to the locus of χ in the Cole-Cole plot was performed to extract the values of χ_{adia}, χ_{iso} and η, using the following equation, independent of τ and of the frequency:

$$\chi'' = \frac{1}{4\cos^2\left(\frac{\pi\eta}{2}\right)}\left(\sqrt{2}\sqrt{\cos^2\left(\frac{\pi\eta}{2}\right)\left(-\cos(\pi\eta)\left(\chi_{adia}+\chi_{iso}-2\chi'\right)^2+4\chi'\left(\chi_{adia}+\chi_{iso}\right)-6\chi_{adia}\chi_{iso}+\chi_{adia}^2+\chi_{iso}^2-4\left(\chi'\right)^2\right)}+\sin(\pi\eta)\left(\chi_{adia}-\chi_{iso}\right)\right)$$

where χ_{adia} and χ_{iso} stand for adiabatic and isothermal susceptibilities respectively and η characterizes the spreading of the relaxation time.

In a second step τ is obtained by the fit of χ' and χ'' using the values of χ_{adia}, χ_{iso} and η determined in the first step:

$$\chi' = \frac{\left(\chi_{iso}-\chi_{adia}\right)\left((2\pi)^{1-\eta}\sin\left(\frac{\pi\eta}{2}\right)(\upsilon\tau)^{1-\eta}+1\right)}{(2\pi)^{2-2\eta}(\upsilon\tau)^{2-2\eta}+2^{2-\eta}\pi^{1-\eta}\sin\left(\frac{\pi\eta}{2}\right)(\upsilon\tau)^{1-\eta}+1}$$

$$\chi'' = \frac{\left(\chi_{iso}-\chi_{adia}\right)(2\pi)^{1-\eta}\cos\left(\frac{\pi\eta}{2}\right)(\upsilon\tau)^{1-\eta}}{(2\pi)^{2-2\eta}(\upsilon\tau)^{2-2\eta}+2^{2-\eta}\pi^{1-\eta}\sin\left(\frac{\pi\eta}{2}\right)(\upsilon\tau)^{1-\eta}+1}$$

The values of τ, η, χ_{adia} and χ_{iso} at the studied temperatures are given in Table S2 in the supporting information. The small η values (η = 0.07−0.13), with respect to that expected for a Debye model (η = 0), indicate a small dispersion of relaxation times.[63]

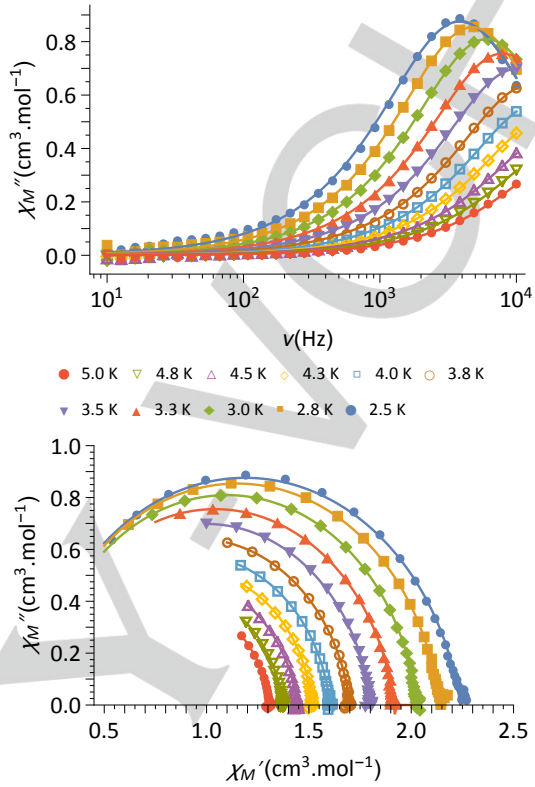

Figure 9. (top) Out-of-phase component, χ_M'', of the magnetic susceptibility of **1** under a 1.8 kOe magnetic field and for frequencies comprised between 10 Hz and 10 kHz. (bottom) Cole–Cole plot of **1** measured from 2.5 to 5 K under 1.8 kOe. The solid lines are the least-squares fitting of the data using a generalized Debye model.

The spin relaxation can occur by several mechanisms,[64,65] namely quantum tunneling, direct, Raman and Orbach processes. The thermal and magnetic field variation of these mechanisms are given in the following equation:

$$\tau^{-1} = AH^4T + \frac{B_1}{1+B_2T} + CT^n + \tau_0^{-1}\exp\left(\frac{-U_{eff}}{kT}\right)$$

where n is the Raman exponent, τ_0 is the pre-exponential factor and U_{eff} is the effective energy barrier to reverse the magnetization.[65] For Kramer's doublet the theoretical n exponent is equal to 9,[66] and the direct process varies with the power 4 of the magnetic field.[64,66]

Accepted Manuscript

This article is protected by copyright. All rights reserved.

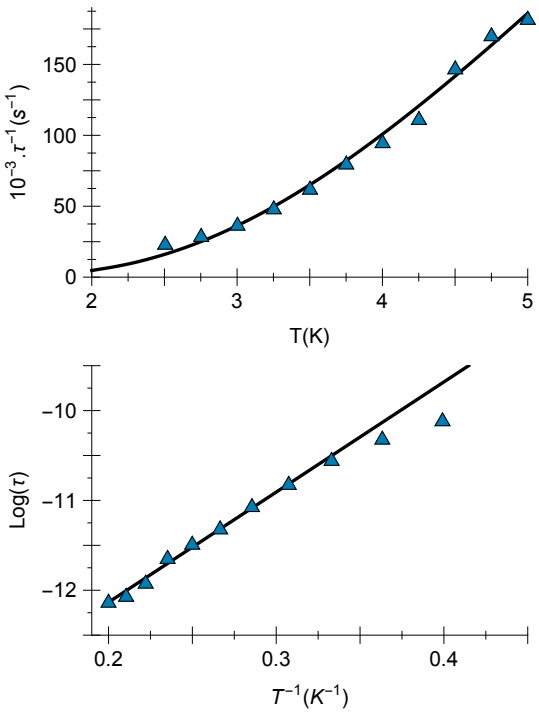

Figure 10. (top) Relaxation Time *1/τ v. T* for complex **1**; (bottom) Log(*τ*) *v. 1/T* for compound **1**. The solid black lines are the best fitting curves.

Obviously, the determination of 6 parameters with a single data set is extremely delicate and almost meaningless due to over-parameterization. In favorable cases, it is possible to determine the three parameters for magnetic field-dependent relaxation mechanisms at low temperatures by measuring the relaxation time as a function of the magnetic field. For this to happen, the Raman and Orbach mechanisms must be negligible at these temperatures. This is the case for the Raman mechanism, which varies according to the power of 9 of the temperature, but for the Orbach one, the energy barrier must be large to fulfill this condition. In the case of **1**, these favorable conditions are not met due to the low blocking temperature, which implies a probable small energy barrier. The determination of the parameters by modeling the *1/τ* curve as a function of the temperature is therefore rather unreliable. Nevertheless, considering that the *Log(τ)* curve as a function of *1/T* is almost linear (Figure 10), we have assumed that the Orbach mechanism is dominant and the equation we have used to fit the data is:

$$\tau^{-1} = \tau_0^{-1}\exp\left(-\frac{U_{eff}}{kT}\right)$$

The best fit parameters are U_{eff} = 8.5 cm^{-1} and τ_0 = 4.6*10^{-7} (Figure 10), with F = 2.5 × 10^{-3}. The deviation from linearity at low temperature for the experimental points in the curve of *Log(τ)* versus *1/T* probably comes from the effect of relaxation mechanisms not considered in the modeling (Figure 10 bottom). The U_{eff} and τ_0 values are in the expected range for SMM compounds. However, these values should be taken with caution because only the Orbach relaxation mechanism has been taken into account.

The magnetic properties of **2** were investigated in the 2 – 300 K temperature range. Two applied field, 1000 Oe and 1 T, were used at low and high temperature, respectively. Its χ_M versus *T* plot is shown in Figure 11. At room temperature, $\chi_M T$ is equal to 0.376 cm^3 mol^{-1} K, a smaller value than the calculated one for an isolated Cu^{II} ion (S_{Cu}^{II} = ½, $\chi_M T$ = 0.413 cm^3 mol^{-1} K with g_{Cu} = 2.1 (inset Figure 11)). This value is typical of an antiferromagnetic behavior arising from an antiferromagnetic interaction between two adjacent Cu(II) ions through the oxamato bridge. A broad maximum of χ_M is observed at 70 K, followed by a minimum and a sharp increase at low temperature. This last feature is due to a small amount of a Cu(II) uncoupled impurity.

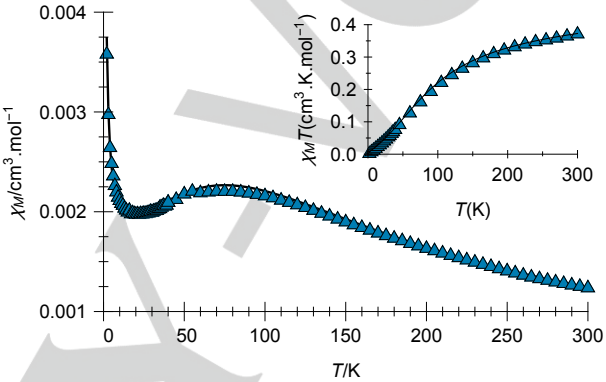

Figure 11. Experimental and best fitting curve of χ_M *vs. T* for **2** under an applied magnetic field of 1 T (T≥ 40 K) and 1000 Oe (T ＜40 K). Inset shows the temperature dependence of $\chi_M T$ for **2**. The solid black lines are the best obtained fit.

To model the magnetic data of **2**, the Bonner Fisher's empirical law for a *S* = 1/2 1D regular chain has been used,[67] to which we have added a TIP contribution (temperature independent paramagnetism) of 60*10^{-6} cm^3 mol^{-1} per Cu^{II} ion. Furthermore, to take into account the small amount of impurity a Curie law term was added:

$$\chi_M = \frac{Ng^2\beta^2}{kT}\frac{0.25+0.074975x+0.075235x^2}{1.0+0.9931x+0.172135x^2+0.757825x^3}(1-\rho)+\left(\frac{Ng^2\beta^2}{4kT}\right)\rho+TIP$$

with:

$$x = \frac{|J|}{kT}$$

N being Avogadro's number, β being the electronic Bohr magneton, *k* is the Boltzmann constant, *J* is magnetic coupling constant and *g* is the gyromagnetic Lande factor. ρ is the mass proportion of uncoupled impurity. The best fit parameters obtained are *J* = -84.1 cm^{-1}, *g* = 2.176, ρ = 0.0033 (Figure 11), with F = 9.14 × 10^{-8}.

In comparison to other oxamate-bridged Cu^{II} homometallic compounds, the result shows a weaker antiferromagnetic interaction in **2**.[68,69] This is due to the particular coordination of the copper ion inside this chain which presents the so-called orbital reversal phenomenon.[70–72] Because of the helical

Accepted Manuscript

This article is protected by copyright. All rights reserved.

structure and the 4+1 copper(II) coordination, the Cu-O2 bond length is the largest. This means that the delocalized spin density onto the O2 oxygen atom is very weak. In fact, the high spin densities are localized on the O1, O3, O4 and N1 atoms, to where the d_{x2-y2} orbital containing the single electron of the Cu^{II} ion points. As such, when compared to the systems where the magnetic d_{x2-y2} orbitals of neighboring copper ions share the same plane with the oxamato bridge, the interaction through the oxamate bridge is much weaker here. It only occurs on the amide function side. This considerably reduces the overlap between the magnetic orbitals of the neighboring magnetic centers. The interaction being approximately proportional to the square of the overlap between magnetic orbitals,[73] a lower overlap results in a lower interaction, as observed in compound **2**. In the helical copper chain obtained with the 2-dimethylaminoethyl(oxamato) ligand, the interaction is equal to -74.1 cm^{-1},[42] close to the value determined for **2**.

Conclusions

The use of the heterotopic hydroxyphenyloxamic ligand in non-aqueous media has led to the formation of two homometallic compounds, a mixed-valence cobalt-based macrocycle and a copper-based chiral 1D polymer. The atypical structures we have obtained with this type of bis-polydentate ligands open up new prospects. An a posteriori analysis of the structures of the two compounds shows that they are not as serendipitous as we originally thought. We will use these findings to investigate both the nature of the additional coordinating group and its position on the phenyloxamate platform.

Experimental Section

All reagents were used as purchased with no further purification. The ester form of the ligand, ethyl *N*-(2-hydroxyphenyl)oxamate, was prepared according the general procedure for oxamate ligand,[74] which differs from the previously reported synthesis.[75]

Ligands preparation. Ethyl *N*-(2-hydroxyphenyl)oxamate (H_2Etohpma). To 5.00 g of 2-aminophenol (M=109.1 $gmol^{-1}$, 45.8 mmol) in 150 mL of THF were added dropwise 5.2 mL of ethyloxalyl chloride (98%; 1eq.) under strong stirring. The mixture was refluxed for 90 min. The resulting dark red solution was left to cool down and filtered on paper. Removal of the solvent under reduced pressure yielded a grey powder. The powder was washed with 400 mL of H_2O under stirring for 30 min and then collected on a sintered glass filter. Further washing was performed rapidly with cold 96% ethanol and the solid was dried with ether and then in air. The final product was collected as a white powder (Yield: 6.36 g, 66% based on the 2-aminophenol; M=209.2 $gmol^{-1}$). ^{1}H-NMR (300 MHz, DMSO) δ (ppm): 10.19 (s, 1H), 9.60 (s, 1H), 7.94 (d, *J* = 8.0 Hz, 1H), 7.02 (t, *J* = 7.4 Hz, 1H), 6.92 (d, *J* = 8.1 Hz, 1H), 6.83 (d, *J* = 7.7 Hz, 1H), 4.29 (q, *J* = 7.1 Hz, 2H), 1.30 (t, *J* = 7.1 Hz, 3H). ^{13}C-NMR (75 MHz, DMSO) δ (ppm): 160.97 (s, -COO-), 154.85 (s, -CONH-), 148.02 (s, Ph), 126.08 (s, Ph), 125.17 (s, Ph), 121.35 (s, Ph), 119.65 (s, Ph), 115.29 (s, Ph), 63.09 (s, $-CH_2-$), 14.29 (s, $-CH_3$). FTIR (cm^{-1}): 3361 (m), 3241 (m), 1723 (m), 1682 (s), 1595 (s), 1540 (s), 1507 (m), 1462 (s), 1397 (s), 1369 (m), 1347 (m), 1326 (m), 1266 (s), 1227 (m), 1188 (m), 1103 (m), 1022 (m), 947 (m), 877 (s), 834 (s), 743 (m), 703 (m), 652 (m), 571 (m), 453 (m), 350 (s). Elemental analysis (%): calc. for $C_{10}H_{11}NO_4$. C, 57.41; H, 5.30; N, 6.70. Found: C, 57.12; H, 5.26; N, 6.71.

***N*-(2-hydoxyphenyl)oxamic acid hydrate, mixed sodium salt ($H_{2.5}Na_{0.5}$-ohpma·0.5H_2O).** To 6.25 g of H_2Et-ohpma (M = 209.2 $gmol^{-1}$; 29.9 mmol) suspended in 400 mL of water were slowly added 45 mL of 2M NaOH (3eq.). The solution was stirred for 30 min and filtered on paper. Under stirring, 23 mL of 4M HCl (3eq.) were added dropwise to the filtrate and stirring was maintained for 1 hr in an ice bath. The precipitate that formed was collected on a sintered glass filter. Further washing was done with cold 96% ethanol and the resulting white solid was dried with ether and then in air. (Yield: 5.66 g, 94% based on H_2Et-ohpma; M=201.1 $gmol^{-1}$). ^{1}H-NMR (400 MHz, DMSO) δ (ppm): 10.36 (s, 1H), 9.81 (s, 1H), 8.09 (d, *J* = 7.9 Hz, 1H), 6.87 (m, 2H), 6.80 (t, *J* = 7.7 Hz, 1H). ^{13}C-NMR (101 MHz, DMSO) δ (ppm): 162.18 (s, -COO-), 158.86 (s, -CONH-), 146.72 (s, Ph), 125.61 (s, Ph), 124.48 (s, Ph), 119.32 (s, Ph), 119.04 (s,Ph), 114.88 (s, Ph). FTIR (cm^{-1}): 3488 (w), 3381 (w), 3076 (s), 1771 (m), 1676 (s), 1612 (m), 1594 (w), 1540 (s), 1469 (s), 1357 (m), 1278 (m), 1192 (w), 1103 (w), 930 (w), 805 (m), 749 (s), 692 (m), 599 (m), 504 (s), 452 (m), 317 (m). Elemental analysis (%): calc. for $C_8H_{7.5}NNa_{0.5}O_{4.5}$. C, 47.77; H, 3.76; N, 6.96. Found: C, 47.94; H, 3.68; N, 6.95.

[$Co_2(H_2O)(O_2CCMe_3)_4(HO_2CCMe_3)_4$], {$Co_2$piv}, was prepared according to the literature procedure.[76] Elemental analysis (%) calculated for $C_{40}H_{78}Co_2O_{17}$ (M_r=948.9 g mol^{-1}): C 50.63, H 8.29. Found: C 50.46, H 8.25.

$(TMA)_3$[{Co^{III}(ohpma)$_2$$Co^{II}$(MeOH)$_2$}$_3$]·10$H_2O$·5MeOH (1). To a 15 mL MeOH solution of $H_{2.5}Na_{0.5}$-ohpma·0.5(H_2O) (0.100 g, 0.5 mmol) was added 690 μL of TMAOH (tetramethylammonium hydroxide 25% w/w in MeOH, 1.5 mmol) and the resulting solution was stirred for 15 min. {Co_2Piv} (0.474 g, 0.5 mmol, M=948.9 $gmol^{-1}$, 1eq.) was then added directly into the solution. The solid {Co_2Piv} dissolved immediately with the apparition of a light precipitate that quickly disappears; giving a red-brown solution. Stirring was maintained for 2 h and the solution was filtered and left to crystallize by slow evaporation at room temperature. Dark brown block crystals of $(TMA)_3$[{Co^{III}(ohpma)$_2$$Co^{II}$(MeOH)$_2$}$_3$]·10$H_2O$·5MeOH (**1**) were obtained overnight (Yield: 0.100 g, 58% based on the ligand; M=2071.1 $gmol^{-1}$). Elemental analysis (%): calc. for $C_{63}H_{100}Co_6N_{10}O_{45}$: C, 36.53; H, 4.87; N, 6.76. Found: C, 36.37; H, 4.81; N, 6.54. Selected IR data (cm^{-1}): 3185(sh), 2929(w), 1602(m), 1465(m), 1421 (w), 1338(m), 1301(w), 1273(s), 1241(m), 1151(w), 1105(w), 1025(w), 962(m), 950(w), 892(m), 844(s), 745(m), 645(w), 607(m), 451(w), 403(m), 329(m), 235(w).

($HNEt_3$)[Cu(ohpma)] (2). To a 15 mL acetonitrile solution of H_2Etohpma (0.104 g, 0.5 mmol) was added 210 μL of NEt_3 (1.5 mmol). A 5 mL aqueous solution of $CuCl_2.2H_2O$ (0.084 g, 0.5 mmol) was then added dropwise. The resulting green solution was kept under stirring for 2 h and then filtered. Green block crystals of ($HNEt_3$)[Cu(ohpma)] (**2**) were obtained after two days by slow evaporation of the solution and washed with acetonitrile (Yield: 0.134 g, 78% based on the ligand; M=343.8 $gmol^{-1}$). Elemental analysis (%): calc. for $C_{14}H_{20}CuN_2O_4$: C, 48.90; H, 5.86; N, 8.15. Found: C, 48.37; H, 5.75; N, 7.90. Selected IR data (cm^{-1}): 2992(w), 1647(m), 1605(s), 1576(m), 1465(s), 1405(m), 1326(m), 1305(m), 1290(m), 1265(s), 1240(s), 1182(m), 1148(m), 1103(w), 1026(w), 878(s), 780(s), 594(m), 557(m), 493(w), 456(w), 336(m).

Magnetic measurements. Magnetic measurements in dc mode were performed on polycrystalline samples of 1 and 2 restrained within a capsule with a Quantum Design MPMS SQUID. Magnetic susceptibility data were corrected for the diamagnetism of the constituent atoms using the Pascal's constants. The diamagnetism of the sample holder was measured and subtracted from the raw data.

Elemental analysis were performed in the "service de microanalyse" at ICSN (CNRS, Gif/Yvette).

Accepted Manuscript

This article is protected by copyright. All rights reserved.

FT-IR, TGA, NMR. ATR/FT-IR spectra were collected on a Bruker TENSOR 27 equipped with a simple reflexion ATR diamond plate of the Harrick MPV2 series. The thermogravimetric analysis (TGA) was performed on a TA Instruments SDTQ600 under air or nitrogen with a heating rate of 5 °C/min. ^{1}H and ^{13}C NMR spectra were collected on 300 and 400 MHz Bruker Avance spectrometers at 298 K.

CD, UV-Vis spectra. Circular dichroism spectra were collected on a JASCO J-815 spectropolarimeter at room temperature, in the solid state using KBr pellets or in solution (MeCN:H_2O). UV-Vis spectra were collected on a Agilent Cary-5000 spectrometer, at room temperature, in the solid state using KBr pellets or in solution (MeCN:H_2O).

Crystallography. Crystal data for **1** ($C_{74}H_{118.50}Co_6N_9O_{39}$): dark blocks, monoclinic, $P2_1/c$, a = 9.9479(3) Å, b = 28.8849(10) Å, c = 32.8203(10) Å, β = 97.123(2), V = 9357.9(5) Å^3, Z = 4, T = 200(2) K, ρ = 1.502 g cm^{-3}, F(000) = 4406, μ = 1.130 mm^{-1}. Crystal data for **2** ($C_{14}H_{20}CuN_2O_4$): green hexagons, trigonal, $P3_2$, a = 9.6625(2) Å, c = 13.9393(4) Å, V = 1127.07(6) Å^3, Z = 3, T = 200(2) K, ρ = 1.520 g cm^{-3}, F(000) = 537, μ = 1.470 mm^{-1}. The data collections for **1** and **2** were carried out on a Bruker Kappa-APEX II CCD diffractometer (MoKα, λ = 0.71073 Å). Crystals were mounted on a cryoloop using Parabar oil and placed in the cold flow produced with an Oxford Cryosystems device. Data collection strategies were generated with the APEX2 suite of programs (BRUKER).[77] The refinement of the unit cell parameters and data reduction were carried out with SAINT (BRUKER),[77] and absorptions were corrected with SADABS.[77,78] The structures were solved with SHELXT-14[79] and refined with the SHELXL-2014/7 program[79] (WinGX or Olex 2 software packages[80,81]). Data refinement for **1** gave (using 1237 parameters and 14 restraint) wR_2 = 0.2039 (18383 unique reflections), R_1 = 0.0898 [14569 reflections with $I > 2\sigma(I)$], and GOF = 1.186. A disorder model (with a ratio of 0.9/0.1) was introduced for the Co2 and Co6 atoms as well as some atoms in their coordination spheres to take into account the residual density in these regions. However, this model is only partial. Further disorder modelling leads unfortunately to either a diverging model or an incomplete one, since the residual density is mostly observed for the Co atoms. Data refinement for **2** gave (using 194 parameters and 1 restraint) wR_2 = 0.0527 (4906 unique reflections), R_1 = 0.0198 [4748 reflections with $I > 2\sigma(I)$], GOF = 1.060, and a Flack parameter of -0.021(3). CCDC-1985070 and 1985071 contain the supplementary crystallographic data for this article. These data can be obtained free of charge from the Cambridge Crystallographic Data Centre via www.ccdc.cam.ac.uk/structures.

Acknowledgments

This work was supported by the Ministère de la Recherche et de l'Enseignement Supérieur (MRES), the Centre National de la Recherche Scientifique (CNRS) and the China Scholarship Council (CSC) in the form of M. Ang Li's PhD fellowship. The authors would like to thank Dr Hani Amouri for the fruitful discussions on chirality, and the staff of the low temperature physical measurement MPBT technical platform at Sorbonne Université.

Keywords: N,O ligands • chiral coordination polymer • macrocycle • magnetic properties • oxamate

[1] T. Grancha, J. Ferrando-Soria, M. Castellano, M. Julve, J. Pasán, D. Armentano, E. Pardo, *Chem. Commun.* **2014**, *50*, 7569–7585.
[2] M. Castellano, R. Ruiz-García, J. Cano, J. Ferrando-Soria, E. Pardo, F. R. Fortea-Pérez, S.-E. Stiriba, W. P. Barros, H. O. Stumpf, L. Cañadillas-Delgado, J. Pasán, C. Ruiz-Pérez, G. de Munno, D. Armentano, Y. Journaux, F. Lloret, M. Julve, *Coord. Chem. Rev.* **2015**, *303*, 110–138.
[3] F. R. Fortea-Pérez, M. Mon, J. Ferrando-Soria, M. Boronat, A. Leyva-Pérez, A. Corma, J. M. Herrera, D. Osadchii, J. Gascon, D. Armentano, E. Pardo, *Nat. Mater.* **2017**, *16*, 760–766.
[4] M. Mon, R. Bruno, J. Ferrando-Soria, D. Armentano, E. Pardo, *J. Mater. Chem. A* **2018**, *6*, 4912–4947.
[5] Y. Journaux, J. Ferrando-Soria, E. Pardo, R. Ruiz-Garcia, M. Julve, F. Lloret, J. Cano, Y. Li, L. Lisnard, P. Yu, H. Stumpf, C. L. M. Pereira, *Eur. J. Inorg. Chem.* **2018**, *2018*, 228–247.
[6] M. Viciano-Chumillas, M. Mon, J. Ferrando-Soria, A. Corma, A. Leyva-Pérez, D. Armentano, E. Pardo, *Acc. Chem. Res.* **2020**, *53*, 520–531.
[7] E. Pardo, R. Ruiz-Garcia, J. Cano, X. Ottenwaelder, R. Lescouëzec, Y. Journaux, F. Lloret, Miguel. Julve, *Dalton Trans.* **2008**, 2780–2805.
[8] M.-C. Dul, E. Pardo, R. Lescouëzec, Y. Journaux, J. Ferrando-Soria, R. Ruiz-Garcia, J. Cano, M. Julve, F. Lloret, D. Cangussu, C. L. M. Pereira, H. O. Stumpf, J. Pasan, C. Ruiz-Perez, *Coord. Chem. Rev.* **2010**, *254*, 2281–2296.
[9] M. Castellano, R. Ruiz-García, J. Cano, J. Ferrando-Soria, E. Pardo, F. R. Fortea-Pérez, S.-E. Stiriba, M. Julve, F. Lloret, *Acc. Chem. Res.* **2015**, *48*, 510–520.
[10] M. Mon, J. Ferrando-Soria, T. Grancha, F. R. Fortea-Pérez, J. Gascon, A. Leyva-Pérez, D. Armentano, E. Pardo, *J. Am. Chem. Soc.* **2016**, *138*, 7864–7867.
[11] M. Mon, J. Ferrando-Soria, M. Verdaguer, C. Train, C. Paillard, B. Dkhil, C. Versace, R. Bruno, D. Armentano, E. Pardo, *J. Am. Chem. Soc.* **2017**, *139*, 8098–8101.
[12] M. Mon, R. Bruno, E. Tiburcio, P.-E. Casteran, J. Ferrando-Soria, D. Armentano, E. Pardo, *Chem. - Eur. J.* **2018**, *24*, 17712–17718.
[13] M. Mon, R. Bruno, E. Tiburcio, A. Grau-Atienza, A. Sepúlveda-Escribano, E. V. Ramos-Fernandez, A. Fuoco, E. Esposito, M. Monteleone, J. C. Jansen, J. Cano, J. Ferrando-Soria, D. Armentano, E. Pardo, *Chem. Mater.* **2019**, *31*, 5856–5866.
[14] E. Pardo, R. Ruiz-García, F. Lloret, J. Faus, M. Julve, Y. Journaux, M. A. Novak, F. S. Delgado, C. Ruiz-Pérez, *Chem. - Eur. J.* **2007**, *13*, 2054–2066.
[15] J. Ferrando-Soria, T. Grancha, M. Julve, J. Cano, F. Lloret, Y. Journaux, J. Pasán, C. Ruiz-Pérez, E. Pardo, *Chem. Commun.* **2012**, *48*, 3539–3541.
[16] T. Grancha, M. Mon, F. Lloret, J. Ferrando-Soria, Y. Journaux, J. Pasán, E. Pardo, *Inorg. Chem.* **2015**, *54*, 8890–8892.
[17] C. O. Paul-Roth, *Comptes Rendus Chimie* **2005**, *8*, 1232–1236.
[18] K. Yoneda, Y. Hori, M. Ohba, S. Kitagawa, *Chem. Lett.* **2008**, *37*, 64–65.
[19] T. L. Oliveira, L. H. G. Kalinke, E. J. Mascarenhas, R. Castro, F. T. Martins, J. R. Sabino, H. O. Stumpf, J. Ferrando, M. Julve, F. Lloret, D. Cangussu, *Polyhedron* **2014**, *81*, 105–114.
[20] K. Rühlig, R. Mothes, A. Aliabadi, V. Kataev, B. Büchner, R. Buschbeck, T. Rüffer, H. Lang, *Dalton Trans.* **2016**, *45*, 7960–7979.
[21] T. S. Fernandes, R. S. Vilela, A. K. Valdo, F. T. Martins, E. García-España, M. Inclán, J. Cano, F. Lloret, M. Julve, H. O. Stumpf, D. Cangussu, *Inorg. Chem.* **2016**, *55*, 2390–2401.
[22] A. Conte-Daban, V. Borghesani, S. Sayen, E. Guillon, Y. Journaux, G. Gontard, L. Lisnard, C. Hureau, *Anal. Chem.* **2017**, *89*, 2155–2162.
[23] T. S. Fernandes, W. D. C. Melo, L. H. G. Kalinke, R. Rabelo, A. K. Valdo, C. C. da Silva, F. T. Martins, P. Amorós, F. Lloret, M. Julve, D. Cangussu, *Dalton Trans.* **2018**, *47*, 11539–11553.
[24] L. Hou, L.-N. Ma, X.-Y. Li, Y.-Z. Li, W.-J. Shi, G. Liu, Y.-Y. Wang, *ChemPlusChem* **2019**, *84*, 62–68.
[25] T. T. da Cunha, V. M. M. Barbosa, W. X. C. Oliveira, C. B. Pinheiro, E. F. Pedroso, W. C. Nunes, C. L. M. Pereira, *Polyhedron* **2019**, *169*, 102–113.
[26] J. Maciel, L. Kalinke, A. Valdo, F. Martins, R. Rabelo, N. Moliner, J. Cano, M. Julve, F. Lloret, D. Cangussu, *J. Braz. Chem. Soc.* **2019**, *30*, 2413–2429.

Accepted Manuscript

This article is protected by copyright. All rights reserved.

[27] T. Grancha, J. Ferrando-Soria, J. Cano, F. Lloret, M. Julve, G. D. Munno, D. Armentano, E. Pardo, *Chem. Commun.* **2013**, *49*, 5942–5944.
[28] W. D. do Pim, É. N. de Faria, W. X. C. Oliveira, C. B. Pinheiro, W. C. Nunes, J. Cano, F. Lloret, M. Julve, H. O. Stumpf, C. L. M. Pereira, *Dalton Trans.* **2015**, *44*, 10939–10942.
[29] D. W. Margerum, *Pure Appl. Chem.* **1983**, *55*, 23–34.
[30] H. Sigel, R. B. Martin, *Chem. Rev.* **1982**, *82*, 385–426.
[31] T. J. Collins, *Acc. Chem. Res.* **1994**, *27*, 279–285.
[32] I. Fernández, J. R. Pedro, A. L. Roselló, R. Ruiz, I. Castro, X. Ottenwaelder, Y. Journaux, *Inorg. Chem.* **2001**, *2001*, 1235–1247.
[33] S. Turner, O. Kahn, L. Rabardel, *J. Am. Chem. Soc.* **1996**, *118*, 6428–6432.
[34] L. Cui, J. Ge, C. F. Leong, D. M. D'Alessandro, J.-L. Zuo, *Dalton Trans.* **2017**, *46*, 3980–3988.
[35] T. Rüffer, B. Bräuer, A. K. Powell, I. Hewitt, G. Salvan, *Inorg. Chim. Acta* **2007**, *360*, 3475–3483.
[36] E.-Q. Gao, J.-K. Tang, D.-Z. Liao, Z.-H. Jiang, S.-P. Yan, G.-L. Wang, *Inorg. Chem.* **2001**, *40*, 3134–3140.
[37] M. V. Marinho, T. R. G. Simões, M. A. Ribeiro, C. L. M. Pereira, F. C. Machado, C. B. Pinheiro, H. O. Stumpf, J. Cano, F. Lloret, M. Julve, *Inorg. Chem.* **2013**, *52*, 8812–8819.
[38] H. O. Stumpf, Y. Pei, O. Kahn, L. Ouahab, D. Grandjean, *Science* **1993**, *261*, 447–449.
[39] E. Pardo, R. Ruiz-García, F. Lloret, J. Faus, M. Julve, Y. Journaux, F. Delgado, C. Ruiz-Pérez, *Adv. Mater.* **2004**, *16*, 1597–1600.
[40] J. Ferrando-Soria, T. Grancha, M. Julve, J. Cano, F. Lloret, Y. Journaux, J. Pasán, C. Ruiz-Pérez, E. Pardo, *Chem. Commun.* **2012**, *48*, 3539–3541.
[41] E. Pardo, C. Train, R. Lescouëzec, Y. Journaux, J. Pasán, C. Ruiz-Pérez, F. S. Delgado, R. Ruiz-Garcia, F. Lloret, C. Paulsen, *Chem. Commun.* **2010**, *46*, 2322.
[42] C. Kachi-Terajima, M. Ishii, T. Saito, C. Kanadani, T. Harada, R. Kuroda, *Inorg. Chem.* **2012**, *51*, 7502–7507.
[43] T. Grancha, X. Qu, M. Julve, J. Ferrando-Soria, D. Armentano, E. Pardo, *Inorg. Chem.* **2017**, *56*, 6551–6557.
[44] L. Pérez-García, D. B. Amabilino, *Chem. Soc. Rev.* **2007**, *36*, 941–967.
[45] L. Han, M. Hong, *Inorg. Chem. Commun.* **2005**, *8*, 406–419.
[46] *Nomenclature of Inorganic Chemistry*, **2005**.
[47] A. Caneschi, D. Gatteschi, P. Rey, R. Sessoli, *Inorg. Chem.* **1991**, *30*, 3936–41.
[48] G. Huang, X. Yi, F. Gendron, B. L. Guennic, T. Guizouarn, C. Daiguebonne, G. Calvez, Y. Suffren, O. Guillou, K. Bernot, *Dalton Trans.* **2019**, *48*, 16053–16061.
[49] A. Caneschi, D. Gatteschi, N. Lalioti, C. Sangregorio, R. Sessoli, G. Venturi, A. Vindigni, A. Rettori, M. G. Pini, M. A. Novak, *Angew. Chem. Int. Ed.* **2001**, *40*, 1760–1763.
[50] A. Lennartson, M. Håkansson, *New J. Chem.* **2015**, *39*, 5936–5943.
[51] D. K. Kondepudi, R. J. Kaufman, N. Singh, *Science* **1990**, *250*, 975–976.
[52] S.-T. Wu, Y.-R. Wu, Q.-Q. Kang, H. Zhang, L.-S. Long, Z. Zheng, R.-B. Huang, L.-S. Zheng, *Angew. Chem. Int. Ed.* **2007**, *46*, 8475–8479.
[53] A. Lennartson, M. Håkansson, *Angew. Chem. Int. Ed.* **2009**, *48*, 5869–5871.
[54] F. Lloret, M. Julve, J. Cano, R. Ruiz-Garcia, Emilio. Pardo, *Inorg. Chim. Acta* **2008**, *361*, 3432–3445.
[55] J. R. Neilson, D. E. Morse, B. C. Melot, D. P. Shoemaker, J. A. Kurzman, R. Seshadri, *Phys. Rev. B* **2011**, *83*, 094418.
[56] J. S. Griffith, *The Theory of Transition-Metal Ions*, Cambridge University Press, Cambridge, **1971**.
[57] M. E. Lines, *J. Chem. Phys.* **1971**, *55*, 2977–2984.
[58] F. Lloret, M. Julve, J. Cano, R. Ruiz-Garcìa, E. Pardo, *Inorg. Chim. Acta* **2008**, *361*, 3432–3445.
[59] N. Ishikawa, M. Sugita, T. Ishikawa, S. Koshihara, Y. Kaizu, *J. Am. Chem. Soc.* **2003**, *125*, 8694–8695.
[60] M. Jeletic, P.-H. Lin, J. J. Le Roy, I. Korobkov, S. I. Gorelsky, M. Murugesu, *J. Am. Chem. Soc.* **2011**, *133*, 19286–19289.
[61] K. S. Cole, R. H. Cole, *J. Chem. Phys.* **1941**, *9*, 341–351.
[62] C. Dekker, A. F. M. Arts, H. W. de Wijn, A. J. van Duyneveldt, J. A. Mydosh, *Phys. Rev. B* **1989**, *40*, 11243–11251.
[63] J. A. Mydosh, *Spin Glasses : An Experimental Introduction*, CRC Press, London, **1993**.
[64] K. N. Shrivastava, *Phys. Stat. Sol. B* **1983**, *117*, 437–458.
[65] J. M. Zadrozny, M. Atanasov, A. M. Bryan, C.-Y. Lin, B. D. Rekken, P. P. Power, F. Neese, J. R. Long, *Chem. Sci.* **2013**, *4*, 125–138.
[66] L. T. A. Ho, L. F. Chibotaru, *Phys. Rev. B* **2018**, *97*, 024427.
[67] J. C. Bonner, M. E. Fisher, *Phys. Rev.* **1964**, *135*, A640–A658.
[68] J. Parreiras, E. N. Faria, W. X. C. Oliveira, W. D. D. Pim, R. V. Mambrini, E. F. Pedroso, M. Julve, C. L. M. Pereira, H. O. Stumpf, *J. Coord. Chem.* **2018**, *71*, 797–812.
[69] E.-Q. Gao, Q.-H. Zhao, J.-K. Tang, D.-Z. Liao, Z.-H. Jiang, S.-P. Yan, *J. Chem. Soc., Dalton Trans.* **2001**, 1537–1540.
[70] J. J. Girerd, O. Kahn, M. Verdaguer, *Inorg. Chem.* **1980**, *19*, 274–276.
[71] H. Tamaki, Z. J. Zhong, N. Matsumoto, S. Kida, M. Koikawa, N. Achiwa, Y. Hashimoto, H. Okawa, *J. Am. Chem. Soc.* **1992**, *114*, 6974–6979.
[72] Y. Journaux, J. Sletten, O. Kahn, *Inorg. Chem.* **1985**, *24*, 4063–4069.
[73] Olivier. Kahn, *Molecular Magnetism.*, VCH Publishers Inc, New York, **1993**.
[74] B. Cervera, J. L. Sanz, M. J. Ibáñez, G. Vila, F. LLoret, M. Julve, R. Ruiz, X. Ottenwaelder, A. Aukauloo, S. Poussereau, Y. Journaux, M. C. Munoz, *J. Chem. Soc., Dalton Trans.* **1998**, 781–790.
[75] F. J. Martínez-Martínez, I. I. Padilla-Martínez, M. A. Brito, E. D. Geniz, R. C. Rojas, J. B. R. Saavedra, H. Höpfl, M. Tlahuextl, R. Contreras, *J. Chem. Soc., Perkin Trans. 2* **1998**, 401–406.
[76] G. Aromi, A. S. Batsanov, P. Christian, M. Helliwell, A. Parkin, S. Parsons, A. A. Smith, G. A. Timco, R. E. P. Winpenny, *Chem. - Eur. J.* **2003**, *9*, 5142–5161.
[77] *BrukerAXS Inc*, **1998**.
[78] R. H. Blessing, *Acta Crystallogr., Sect. A* **1995**, *51*, 33.
[79] G. M. Sheldrick, *Acta Crystallogr., Sect. C* **2015**, *71*, 3–8.
[80] L. J. Farrugia, *J. Appl. Cryst.* **2012**, *45*, 849–854.
[81] O. V. Dolomanov, L. J. Bourhis, R. J. Gildea, J. a. K. Howard, H. Puschmann, *J Appl Cryst* **2009**, *42*, 339–341.

Accepted Manuscript

This article is protected by copyright. All rights reserved.

10.1002/ejic.202000490

WILEY-VCH

Entry for the Table of Contents (Please choose one layout)

Layout 1:

FULL PAPER

The reaction of a double-sided bis-polydentate oxamate-based ligand with transition metal ions has led to a cobalt-based hexametallic and macrocyclic complex and a copper-based chiral chain compound. Both structural types are not commonly seen in oxamate chemistry and result from the alternative choice of ligand.

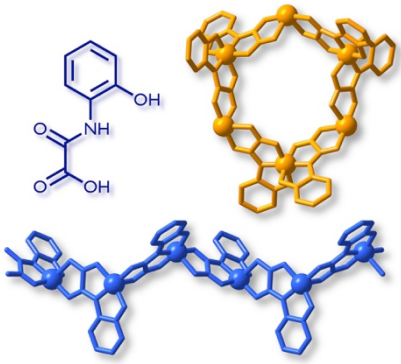

Oxamate chemistry

Ang Li, Yanling Li, Lise-Marie Chamoreau, Christophe Desmarets, Laurent Lisnard and Yves Journaux**

Page No. – Page No.

A bis-polydentate oxamate-based achiral ligand able to stabilize a macrocyclic mixed valence compound or induce a 1D helical chain

WILEY-VCH
Accepted Manuscript

This article is protected by copyright. All rights reserved.